Check for updates

Earth's Future

RESEARCH ARTICLE
10.1029/2024EF005246

Enhancing Urban Thermal Environment and Energy Sustainability With Temperature-Adaptive Radiative Roofs

Keer Zhang[1,2], Lei Zhao[3], Keith Oleson[4], Xinchang "Cathy" Li[3], and Xuhui Lee[1]

[1]School of the Environment, Yale University, New Haven, CT, USA, [2]High Meadows Environmental Institute, Princeton University, Princeton, NJ, USA, [3]Department of Civil and Environmental Engineering, University of Illinois at Urbana-Champaign, Urbana, IL, USA, [4]NSF National Center for Atmospheric Research, Boulder, CO, USA

Abstract Urban overheating presents significant challenges to public health and energy sustainability. Conventional radiative cooling strategies, such as cool roofs with high albedo, lead to undesired winter cooling and increased space heating demand for cities with cold winters, a phenomenon known as heating energy penalty. A novel roof coating with high albedo and temperature-adaptive emissivity (TAE)—low emissivity during cold conditions and high emissivity during hot conditions—has the potential to mitigate winter heating energy penalty. In this study, we implement this roof coating in a global climate model to evaluate its impact on air temperature and building energy demand for space heating and cooling in global cities. Adopting roofs with TAE increases global urban air temperature by up to +0.54°C in the winter (99th percentile; mean change +0.16°C) but has negligible effects on summer urban air temperature (mean change +0.05°C). Combining TAE with high albedo effectively provides summer cooling and does not increase building energy demand in the winter, particularly for mid-latitude cities. Sensitivities of air temperature to changes in emissivity and albedo are associated with local "apparent" net longwave radiation and incoming solar radiation, respectively. We propose a simple parameterization of air temperature responses to emissivity and albedo to facilitate the development of city-specific radiative mitigation strategies. This study emphasizes the necessity of developing mitigation approaches specific to local cloudiness.

Plain Language Summary Traditional cool roofs with high albedo generate cooling all year around, leading to increased energy demand for heating during cold winter. To address this issue, we evaluate a new roof material with high albedo and temperature-adaptive emissivity (TAE) that adjusts its emissivity to provide cooling under hot conditions and heating under cold conditions. Using a global climate model, we find that cities in temperate and arid climates benefit the most from roofs with TAE and high albedo as they provide cooling in summer and warming in winter, thus reducing annual energy usage. Our research calls for tailoring urban climate adaptation strategies to local climate conditions.

Key Points:

- Roofs with temperature-adaptive emissivity (TAE) raise urban winter temperature by 0.16°C on average and up to 0.54°C (99th percentile)
- Mid-latitude cities benefit from roofs with TAE & high albedo, experiencing summer cooling and minimal winter heating energy penalty
- A simple parameterization accurately predicts air temperature response to urban emissivity and albedo

Supporting Information:

Supporting Information may be found in the online version of this article.

Correspondence to:

K. Zhang,
keer.zhang@yale.edu;
kz7693@princeton.edu

Citation:

Zhang, K., Zhao, L., Oleson, K., Li, X. "C"., & Lee, X. (2025). Enhancing urban thermal environment and energy sustainability with temperature-adaptive radiative roofs. *Earth's Future*, *13*, e2024EF005246. https://doi.org/10.1029/2024EF005246

Received 27 AUG 2024
Accepted 9 DEC 2024

Author Contributions:

Conceptualization: Keer Zhang, Lei Zhao, Xuhui Lee
Formal analysis: Keer Zhang
Investigation: Keer Zhang, Lei Zhao, Keith Oleson, Xinchang "Cathy" Li, Xuhui Lee
Methodology: Keer Zhang, Lei Zhao, Keith Oleson, Xinchang "Cathy" Li, Xuhui Lee
Software: Keith Oleson, Xinchang "Cathy" Li
Supervision: Xuhui Lee
Visualization: Keer Zhang
Writing – original draft: Keer Zhang, Xuhui Lee

© 2025. The Author(s).
This is an open access article under the terms of the Creative Commons Attribution-NonCommercial-NoDerivs License, which permits use and distribution in any medium, provided the original work is properly cited, the use is non-commercial and no modifications or adaptations are made.

1. Introduction

The combination of global warming and urban heat islands threatens public health and society's well-being. Urban overheating causes a range of problems, including labor productivity reduction, economic loss, and health burdens (Wang et al., 2023; Zander et al., 2015; Zhao et al., 2021). Meanwhile, addressing climate change and achieving Paris Climate Goals require an effort to improve building energy efficiency, as one-sixth of global energy consumption is attributed to space heating and cooling (Cabeza et al., 2022; IEA, 2019). The energy for cooling is projected to increase by 12 times from 2000 to 2050 due to unmitigated climate change and income increase (Isaac & Vuuren, 2009).

The deterioration of the thermal environment and the increase in energy consumption call for solutions that provide all-year around thermal regulation and energy saving. However, current mitigation efforts are inadequate. Passive radiative cooling (PRC) surfaces with high albedo and high emissivity, such as cool roof and reflective pavement, can reduce ambient temperatures by up to 0.61°C per 0.1 increase of albedo (Santamouris, 2014; Sinsel et al., 2021). Other novel materials, such as retroreflective (X. Huang et al., 2024) and fluorescent materials (Santamouris & Yun, 2020) can also provide cooling and reduce summer cooling load. However, having static radiative properties, these materials also generate undesired winter cooling and may increase space heating during cold seasons, a phenomenon known as heating energy penalty (Khan et al., 2021; K. W. Oleson, Bonan, & Feddema, 2010; Oleson, Bonan, Feddema, Vertenstein, & Kluzek, 2010; Synnefa et al., 2007; Tan et al., 2023).

Writing – review & editing: Keer Zhang, Lei Zhao, Keith Oleson, Xinchang "Cathy" Li, Xuhui Lee

An experimental study in Shanghai, China with hot summer and cold winter shows that reflective building coating reduces annual building cooling electricity demand by 116 kWh, while increases the heating demand by 327 kWh (Shen et al., 2011). Consequently, annual building energy consumption may be increased by PRC surfaces (Feng et al., 2022; K. W. Oleson, Bonan, & Feddema, 2010; Oleson, Bonan, Feddema, Vertenstein, & Kluzek, 2010; Shen et al., 2011), particularly in cities with pronounced diurnal and seasonal climate variations. Previous studies on PRC surfaces have primarily focused on their impact on summer temperature and cooling loads but have not evaluated their effects on climate and energy consumptions in an all-year perspective.

Recent advancements in materials science introduce a temperature-adaptive radiative coating as a potential solution (Tang et al., 2021). This coating has a fixed high albedo of 0.75, but exhibits temperature-adaptive emissivity (TAE), switching from a low emissivity under cold conditions to a high emissivity under hot conditions. The dynamic roof emissivity mitigates the extreme high or low roof temperature by altering the net longwave radiation flux. As a novel, engineering material, the real-world benefits of this TAE coating are yet to be investigated.

A numerical simulation has demonstrated the superiority of TAE roofs with high albedo over traditional roofs in terms of annual energy saving for US cities (Tang et al., 2021). However, this evaluation was based on a simplistic adiabatic approximation assuming thermal equilibrium on a surface, a negligible heat exchange between urban structures, and a simplified longwave radiation process. To understand the real-world benefits, it is essential to couple this novel roof with an urban canyon structure and express the longwave radiation balance explicitly in a real atmosphere. As surface emissivity increases, it simultaneously enhances longwave radiation emission and absorption of the downwelling longwave radiation. The degree to which these two offset each other remains unknown. Moreover, the simulations of Tang et al. (2021) are limited to US cities. The effectiveness of TAE roofs in other climates remains unclear.

This study aims to (a) investigate the impact of TAE roofs on surface climate and building energy demand and (b) evaluate the performance of roofs with TAE and relatively high albedo (0.75) for global cities. The Community Terrestrial Systems Model Version 5.2 (CTSM5.2) with a recently improved building energy model (BEM) is used (Li et al., 2024; K. W. Oleson & Feddema, 2020). Section 2 introduces the temperature-adaptive radiative coating, the global climate model, and the experiment design. Three sets of experiments are conducted to isolate the impacts of TAE, increased albedo, as well as high albedo-TAE combination, on air temperature and on building energy demand for space heating and cooling. Results are presented in Section 3, focusing on the impact of TAE roofs on energy balance and how local climate shapes the air temperature response to emissivity. Section 4 discusses climate-specific radiative roof choices, potential climate impact of adjusting TAE roof properties, and limitations. Finally, Section 5 provides the conclusions. This study offers insights into roof material choice with both health and sustainability benefits for global cities.

2. Materials and Methods

2.1. Temperature-Adaptive Radiative Coating

The temperature-adaptive radiative coating was designed to mitigate the overcooling issue of conventional PRC coats with constant albedo and emissivity (Tang et al., 2021). This coating is developed based on metal-insulator transition of the $W_xV_{1-x}O_2$ alloy, which is synthesized by doping Vanadium Dioxide (VO_2) with tungsten (W). The W fraction (x) was set to be 1.5% so that this material undergoes the metal-insulator transition at a transition temperature of 22°C. A multilayer structure design enables the coating to transition from a low sky-window (or thermal atmospheric window, wavelength from 8 to 13 μm) emissivity of 0.2 for warming at low temperatures, to a high sky-window emissivity of 0.9 for cooling at high temperatures. The gradual phase change occurs between two temperature thresholds: a low temperature threshold (T_1) below which the emissivity is 0.2, and a high temperature threshold (T_2) above which the emissivity is 0.9. The T_1 and T_2 are estimated to be 19°C and 27°C according to measurement from Tang et al. (2021), and the albedo of this material is 0.75, a value optimized for all-season energy saving in major US cities.

We implemented the TAE roofs in the global urban areas in the CTSM, an updated version of the land model of the Community Earth System Model (CESM, Danabasoglu et al., 2020; Lawrence et al., 2019). Since the default roof emissivity in CTSM is already quite high—it is at 0.92 for most regions, the TAE roof emissivity in the high-emissivity state is increased to 0.98 from 0.90 to avoid undesired warming in hot weathers. In addition, CTSM

23284277, 2025, 1, Downloaded from https://agupubs.onlinelibrary.wiley.com/doi/10.1029/2024EF005246 by Readcube (Labtiva Inc.), Wiley Online Library on [01/02/2025]. See the Terms and Conditions (https://onlinelibrary.wiley.com/terms-and-conditions) on Wiley Online Library for rules of use; OA articles are governed by the applicable Creative Commons License

23284277, 2025, 1, Downloaded from https://agupubs.onlinelibrary.wiley.com/doi/10.1029/2024EF005246 by Readcube (Labtiva Inc.), Wiley Online Library on [01/02/2025]. See the Terms and Conditions (https://onlinelibrary.wiley.com/terms-and-conditions) on Wiley Online Library for rules of use; OA articles are governed by the applicable Creative Commons License

uses broadband longwave emissivity instead of sky-window emissivity. With these two modifications, in our model runs, the broadband roof emissivity (ε_r) is set at 0.2 or 0.98 when the roof temperature ($T_{s,roof}$) is lower than 19°C or higher than 27°C, respectively, in all cities. When the $T_{s,roof}$ is between 19 and 27°C, ε_r is calculated with a linear interpolation (Figure S1 in Supporting Information S1)

$$\varepsilon_r = 0.0975\ T_{s,roof} - 1.6525 \quad (1)$$

We modified CTSM to update roof emissivity based on roof temperature at every time step (30 min).

2.2. Model Experiments

In CTSM, each grid cell contains up to five land units (lake, glacier, urban, crop, and natural vegetation). Urban areas in CTSM are modeled using the concept of a street canyon, consisting of a roof, sunlit and shaded walls, and pervious and impervious floors. The non-urban near-surface air temperature is interpolated from surface and atmospheric temperatures based on the Monin-Obukhov similarity theory. In urban canyons, the near surface air temperature is determined by solving a series of equations describing the heat exchange between the urban surfaces, the bulk urban canyon air mass, and the atmosphere above (D. Lawrence et al., 2018; K. W. Oleson, Bonan, & Feddema, 2010; Oleson, Bonan, Feddema, Vertenstein, & Kluzek, 2010). CTSM considers 33 unique urban regions, which are grouped according to similar urban properties. Our simulations use a constant urban land cover from Gao and O'Neill (2020) fixed at year 2010. A present-day (circa-2000) urban property data set from Jackson et al. (2010) is adopted to prescribe the default morphology, radiative, and thermal properties of each urban region. The default roof emissivity (ε_d) is about 0.92 for most regions, with exceptions in some urban clusters in Central Asia and Southern South America. These regions have biased-low emissivity (<0.2) and thus are excluded from our analysis to avoid exaggerating summer cooling and underestimating winter warming effect of the TAE roofs. The default roof albedo (α_d) ranges from 0.1 to 0.3 (K. W. Oleson & Feddema, 2020). The BEM of CTSM explicitly simulates interior temperatures by accounting for ventilation, heat conduction through building walls and roofs, sensible heat and longwave radiation exchange between interior surfaces and indoor air. The anthropogenic heat flux is parameterized by a physics-based method using an idealized space heating and air conditioning submodel (K. W. Oleson & Feddema, 2020). This submodel accounts for energy required to maintain indoor temperature within a preset range and waste heat due to equipment inefficiency and energy lost in the conversion of primary energy sources to end use energy. A previous version of CTSM, Community Land Model (CLM) Version 5, models Air Conditioning (AC) adoption implicitly by combining the building thermostat setpoint and AC adoption rate as a proxy for maximum interior building setpoints (K. W. Oleson & Feddema, 2020). For many non-US countries, the proxy maximum interior building setpoints are too high, causing an underestimation of the AC adoption rate and the AC energy flux. CTSM Version 5.2 has adopted a new explicit AC scheme that sets building thermostat setpoint explicitly and uses an updated AC adoption rate data set derived from field surveys and the published literature (Li et al., 2024). This scheme improves the modeled AC energy flux in both its magnitude and spatial distribution.

CLM has been widely used to simulate the climate impact of white roofs (K. W. Oleson, Bonan, & Feddema, 2010; Oleson, Bonan, Feddema, Vertenstein, & Kluzek, 2010; L. Wang et al., 2020; J. Zhang et al., 2016). The urban model of CLM has also been validated extensively against flux tower, site observations, and satellite data (Lipson et al., 2023; K. W. Oleson & Feddema, 2020; K. Zhang et al., 2023; L. Zhao et al., 2014).

The surface energy balance calculation of CTSM accounts for the effects of snow on roofs and roads (D. Lawrence et al., 2018). The fraction of snow cover (f_s) is modeled by calculating the snow accumulation and depletion with a parameterization from Bonan (1996). Roofs and roads can be covered by snowpack in the winter. The emissivity of a snow-covered surface is a weighted combination of the surface emissivity and the snow emissivity (0.97). The urban-scale emissivity change ($\Delta\varepsilon$) caused by TAE roofs is calculated as:

$$\Delta\varepsilon = (\varepsilon_r - \varepsilon_d) \times (1 - f_{s,r}) \times f_r \quad (2)$$

where ε_d and f_r are the default roof emissivity and the roof fraction of the urban land tile and $f_{s,r}$ is the fraction of roof covered by snow. Changes in urban emissivity influence surface climate by perturbing the net longwave radiation (L_n):

23284277, 2025, 1, Downloaded from https://agupubs.onlinelibrary.wiley.com/doi/10.1029/2024EF005246 by Readcube (Labtiva Inc.), Wiley Online Library on [01/02/2025]. See the Terms and Conditions (https://onlinelibrary.wiley.com/terms-and-conditions) on Wiley Online Library for rules of use; OA articles are governed by the applicable Creative Commons License

Table 1
Summary of Experiment Design

Case	Roof emissivity	Roof albedo
Current climate (2010–2012)		
DEF2010	Default	Default
TAE2010	Temperature-adaptive emissivity (0.2–0.98)	Default
TAE&high albedo2010	Temperature-adaptive emissivity (0.2–0.98)	0.75
Future climate (2097–2099)		
DEF2097	Default	Default
TAE2097	Temperature-adaptive emissivity (0.2–0.98)	Default
TAE&high albedo2097	Temperature-adaptive emissivity (0.2–0.98)	0.75

$$L_n = \varepsilon L_{\downarrow} - \varepsilon\sigma T_s^4 \tag{3}$$

where the $L_{\downarrow}$ is downward longwave radiation, T_s is the urban surface temperature, and σ is the Stefan-Boltzmann constant.

Similarly, the urban albedo change ($\Delta\alpha$) induced by high albedo roofs is computed as the difference between its fixed high albedo (0.75) and default roof albedo (α_d), scaled by $1 - f_{s,r}$ and f_r, as:

$$\Delta\alpha = (0.75 - \alpha_d) \times \left(1 - f_{s,r}\right) \times f_r \tag{4}$$

Here, ε_d, α_d, and f_r are known properties from the prescribed surface data, and ε_r and $f_{s,r}$ are modeled by CTSM. Equations 2 and 4 imply the approximation that changing roof material does not influence snow fraction. When roofs are fully covered by snow, the emissivity or albedo of roof material has no effect on the urban microclimate.

As summarized in Table 1, we conducted three experiments using CTSM at a 0.9° latitude × 1.25° longitude grid resolution under the current climate (2010–2012), one with default roof material of CTSM (DEF2010), one with TAE roofs and CTSM default albedo (TAE2010), and the third with TAE roofs and constant high roof albedo of 0.75 (TAE&high albedo2010). These experiments are land-only simulations, driven by the same atmospheric forcing from the Global Soil Wetness Project (GSWP3) data set from 2010 to 2012 (D. M. Lawrence et al., 2019). The factorial experiment design allows us to isolate the impacts of temperature-adaptive emissivity (TAE2010 minus DEF2010), increased albedo (TAE&high albedo2010 minus TAE2010), as well as the combination of TAE and high albedo (TAE&high albedo2010 minus DEF2010). The control simulation with default roof materials was run for 25 years driven by looping over GSWP3 data from 2008 to 2012 as a spin-up to provide the land initial condition for the three experiments.

To assess the effectiveness of these roof materials under climate change, we repeated the three experiments for future climate (2097–2099) under the SSP5-RCP85 scenario, named as DEF2097, TAE2097, and TAE&high albedo2097 (Table 1). The atmospheric forcing was provided by atmospheric output of a fully-coupled CMIP6 simulation conducted by CESM2. The land initial condition was spun up by running the simulation with default roof material driven by looping over atmospheric forcing from 2095 to 2099 for 25 years.

In the following, summer (June–August in the Northern Hemisphere and December–February in the Southern Hemisphere), winter (December–February in the Northern Hemisphere and June–August in the Southern Hemisphere), and annual results are presented. The current climate results are analyzed unless stated otherwise.

3. Results

3.1. Air Temperature Responses to Roofs With TAE and High Albedo

Roofs with TAE have minimal impact on summer urban temperature but produce a notable warming in the winter for most cities (Figures 1c and 1d). During the summer under the current climate, the change in urban temperature (ΔT_a) induced by TAE roofs is a small positive value north of 25°N and south of 25°S (latitudinal mean <0.1°C)

10.1029/2024EF005246

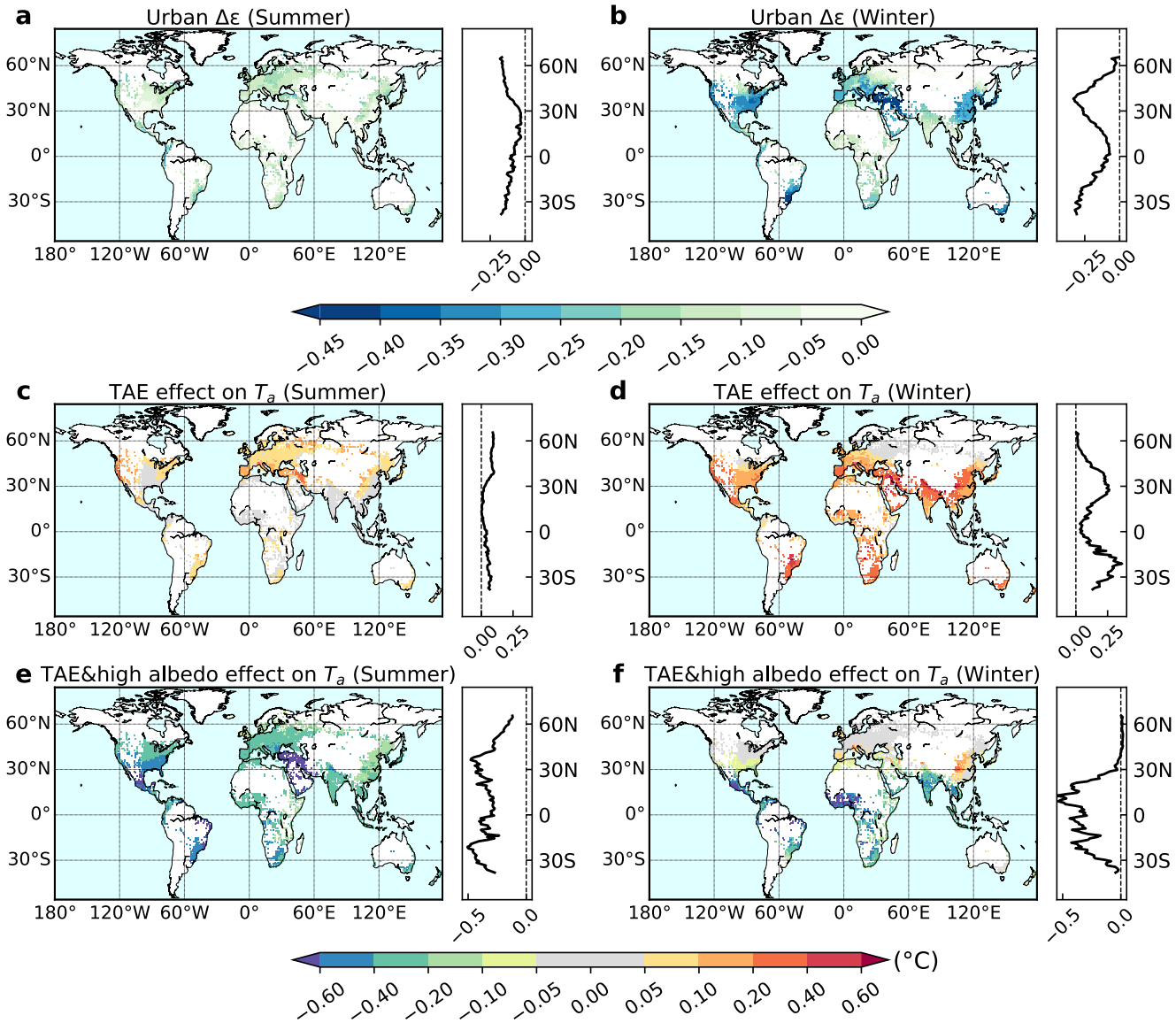

Figure 1. Maps showing changes in urban emissivity (a, b) and urban air temperature (c, d) caused by temperature-adaptive emissivity (TAE) roof, and changes in urban air temperature caused by TAE and high albedo roofs (e, f) under the current climate conditions. Also shown are zonal mean variations.

and is negligible in tropical regions (Figure 1c). In the tropics, the emissivity of TAE roofs is always high (0.7–0.9) due to the high ambient temperature. This emissivity is close to the CTSM default (0.92); the urban emissivity change is too small to cause discernible temperature effects (Figure 1a). The extratropical cities may experience cool nights in the summer, with a mean nighttime $T_{s,roof}$ of about 20°C. In response, TAE roofs switch their emissivity to lower values than the CTSM default. The result is a mild summer warming for mid- and high-latitude cities (mean change +0.07°C north of 25°N; Figure 1c). However, it is worth noting that TAE roofs change summer daily maximum temperature little for most cities (mean change −0.01°C; Figure S2a in Supporting Information S1).

During winter, the influence of TAE roofs on emissivity and air temperature near the equator remains minimal because of the prevailing hot climate (Figures 1b and 1d). The zonal mean ΔT_a shows two peaks of +0.25 and +0.35°C around 30°N and 30°S, respectively. At these latitudes, TAE roofs cause the zonal mean urban emissivity to be 0.2 to 0.3 lower than the CTSM default. Reduced urban emissivity increases urban net longwave radiation flux, which further enhances sensible heat flux and leads to near surface warming (Figures 2 and S4 in

23284277, 2025, 1, Downloaded from https://agupubs.onlinelibrary.wiley.com/doi/10.1029/2024EF005246 by Readcube (Labtiva Inc.), Wiley Online Library on [01/02/2025]. See the Terms and Conditions (https://onlinelibrary.wiley.com/terms-and-conditions) on Wiley Online Library for rules of use; OA articles are governed by the applicable Creative Commons License

10.1029/2024EF005246

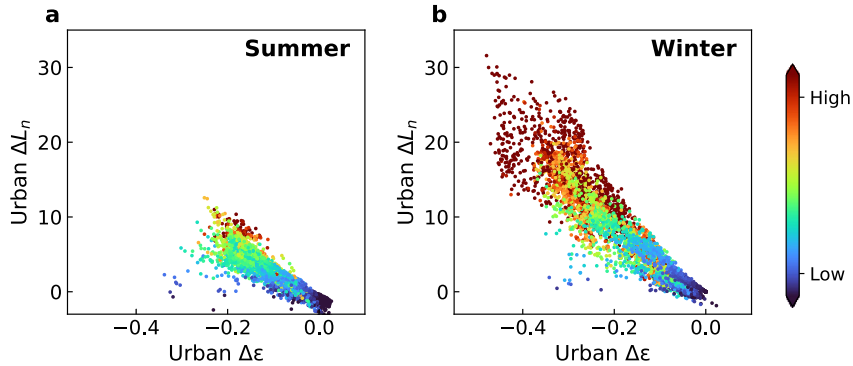

Figure 2. Scatter plots between changes in urban emissivity and urban net longwave radiation (W m^{-2}) induced by temperature-adaptive emissivity (TAE) roofs under the current climate conditions. Each data point represents one urban grid and is colored by TAE effect on air temperature.

Supporting Information S1). Interestingly, for high latitude cities (north of 50°N) experiencing an even colder climate, although TAE roofs have very low emissivity of 0.2, the warming is much weaker (latitudinal mean < +0.07°C) than at mid latitudes. There are two reasons. First, because of snow cover on roofs, the urban emissivity reduction is small (latitudinal mean < +0.15; Figures 1b and S3b in Supporting Information S1). Second, the winter air temperature is not sensitive to emissivity change in these cities at high latitudes due to high cloud cover (Sudmanns et al., 2020). Overall, TAE roofs offer significant winter warming for most cities, increasing daily air temperature by a mean value of +0.16°C and by up to +0.54°C (99th percentile) across global cities.

A drawback of TAE roofs is that they cannot provide summer cooling, which is essential to mitigate dangerous heat risk. High albedo achieves significant cooling, but winter cooling is undesirable. These drawbacks can be overcome by roofs with both TAE and high albedo: summer cooling is retained, and winter heating penalty is avoided or reduced.

In the summer, the cooling effect of high albedo is more than enough to offset the slight warming effect of TAE (Figures 1e and S5c in Supporting Information S1), with evident overall temperature reduction (0.3 to 0.5°C) in tropical and mid-latitude regions and weak cooling in latitudes above 45°N.

In the winter, the albedo cooling continues to dominate in low latitudes (Figures 1f and S5d in Supporting Information S1). In mid-latitude regions, albedo cooling and TAE warming exhibit similar magnitudes (ranging from 0.1 to 0.5°C) but opposite signs, resulting in a near-zero combined effect. At these latitudes, the undesired winter cooling caused by albedo is offset by TAE. For cities north of 50° N, the temperature change is still near zero due to the high snow cover fraction and weak air temperature sensitivities to TAE and albedo.

Regionally, TAE alone changes summer air temperature slightly by −0.01 to +0.12°C, while TAE combined with high roof albedo leads to significant summer cooling of 0.20 to 0.78°C (Figure 3a). The most pronounced cooling is observed in two arid regions, Central Asia and Middle East (−0.68 and −0.78°C). During the winter, the albedo cooling is stronger than the TAE warming in tropical regions, such as Central America, the Amazon Basin, North Africa, and Southeast Asia, resulting in an overall temperature change of −0.29 to −0.47°C (Figure 3b). These hot regions require cooling throughout the year and benefit the most from high albedo effect alone (winter ΔT_a: −0.33 to −0.59°C). For other regions, the combined effect represents a close balance between TAE warming and albedo cooling. The TAE warming fully offsets the albedo cooling in Central Asia, the Mediterranean Coast, East Asia, Australia, the Southern North America, Europe and Northern North America, resulting in a near-zero combined effect.

From a thermal comfort perspective, hot and cold extremes are determined by daily maximum temperature in the summer and daily minimum temperature in the winter, respectively. The summer daily maximum temperature is unaffected by TAE but is reduced greatly by albedo (−0.56 to −1.68°C; Figure S2a in Supporting Information S1). Conversely, the winter daily minimum temperature is affected little by albedo but is significantly increased by TAE (+0.01 to +0.45°C; Figure S2b in Supporting Information S1). This seasonal asymmetry indicates that TAE and high albedo roofs together can reduce both hot and cold extremes for most regions.

23284277, 2025, 1, Downloaded from https://agupubs.onlinelibrary.wiley.com/doi/10.1029/2024EF005246 by Readcube (Labtiva Inc.), Wiley Online Library on [01/02/2025]. See the Terms and Conditions (https://onlinelibrary.wiley.com/terms-and-conditions) on Wiley Online Library for rules of use; OA articles are governed by the applicable Creative Commons License

10.1029/2024EF005246

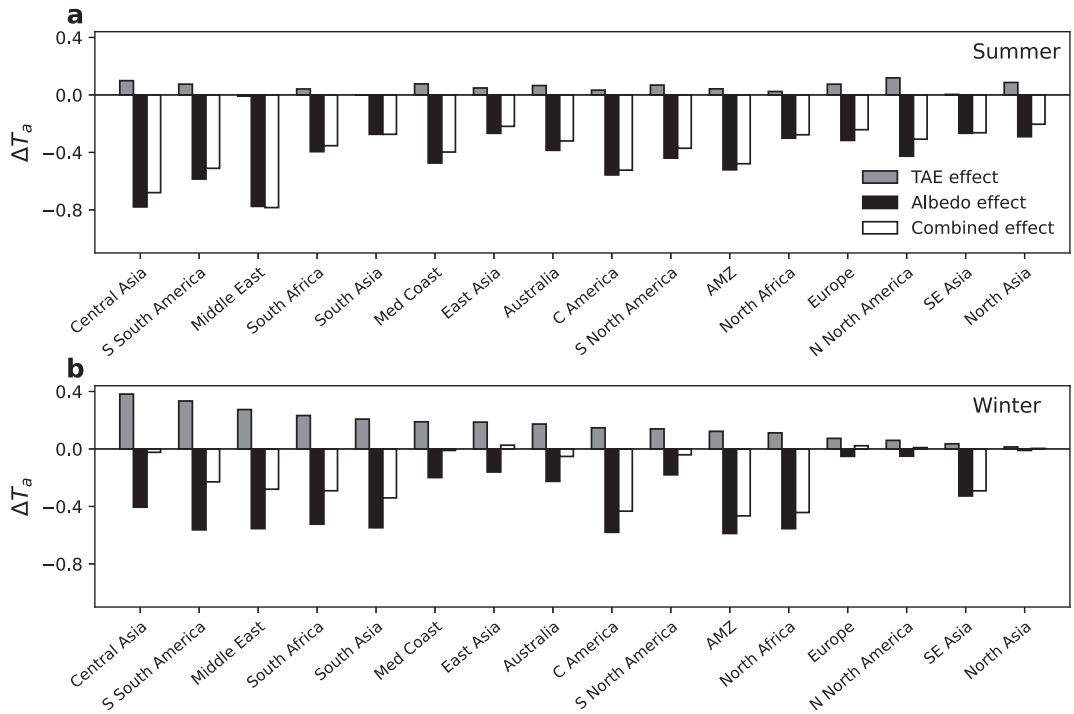

Figure 3. Regional changes in urban air temperature (°C) in the summer (a) and in the winter (b) under the current climate. Region definitions and geographic boundaries are given in Figure S3 in Supporting Information S1.

The TAE roof emissivity and roof surface temperature influence each other in a two-way interaction, and this TAE-$T_{s,roof}$ feedback acts to stabilize the roof temperatures. For instance, at low temperatures, the roof emissivity decreases to provide warming, and the increased roof temperature induced by TAE effect may in turn increase roof emissivity and weaken the initial warming, forming negative feedback to stabilize roof temperatures. But this feedback loop plays a minor role in diurnal variations of urban air temperature (Text S1 in Supporting Information S1).

In the future, TAE roofs generally lead to less warming than in the current climate (Figure S7b in Supporting Information S1). The summer temperature response to TAE becomes close to zero in most cities as future summers are warmer everywhere. In the winter, the roof emissivity change becomes less negative than in the current climate, leading to less TAE warming for most latitudes (Figures S7a and S7b in Supporting Information S1). As for the albedo effect, the summer cooling remains largely unchanged, while winter cooling is reduced by 0.05 to 0.3°C near 20°N and 20°S in comparison to the current climate (Figure S7c in Supporting Information S1). The combined effect of TAE and high albedo changes little in the future (Figure S7d in Supporting Information S1).

3.2. Climate Sensitivity to Emissivity and Albedo

Here, the climate sensitivity is defined as the urban air temperature response to a unit change of urban emissivity ($\Delta T_a/\Delta\varepsilon$) or albedo ($\Delta T_a/\Delta\alpha$). We hypothesize that TAE roofs are more effective in drier regions with less cloud cover and lower humidity. Taking the current climate results as an example, the geographical distribution of $\Delta T_a/\Delta\varepsilon$ supports this hypothesis, showing a more negative $\Delta T_a/\Delta\varepsilon$ in drier cities (Figures 4a, 4c, and 4e). During the summer, the most negative $\Delta T_a/\Delta\varepsilon$ (−1.2 to −1.6°C) is observed in the Western US, the Mediterranean Coast, and Middle East, regions characterized by low humidity and low cloudiness. Conversely, in tropical cities with high cloud cover, $\Delta T_a/\Delta\varepsilon$ is close to zero. In the winter, many regions between 30° N and 30° S, including South Asia, Middle East, North Africa, South Africa, experience a dry season with low cloud cover (Sudmanns et al., 2020), and therefore negative $\Delta T_a/\Delta\varepsilon$ (−1 to −2°C). In contrast, near-zero $\Delta T_a/\Delta\varepsilon$ is observed in Southeast Asia and in latitudes higher than 45° N in the winter.

23284277, 2025, 1, Downloaded from https://agupubs.onlinelibrary.wiley.com/doi/10.1029/2024EF005246 by Readcube (Labtiva Inc.), Wiley Online Library on [01/02/2025]. See the Terms and Conditions (https://onlinelibrary.wiley.com/terms-and-conditions) on Wiley Online Library for rules of use; OA articles are governed by the applicable Creative Commons License

10.1029/2024EF005246

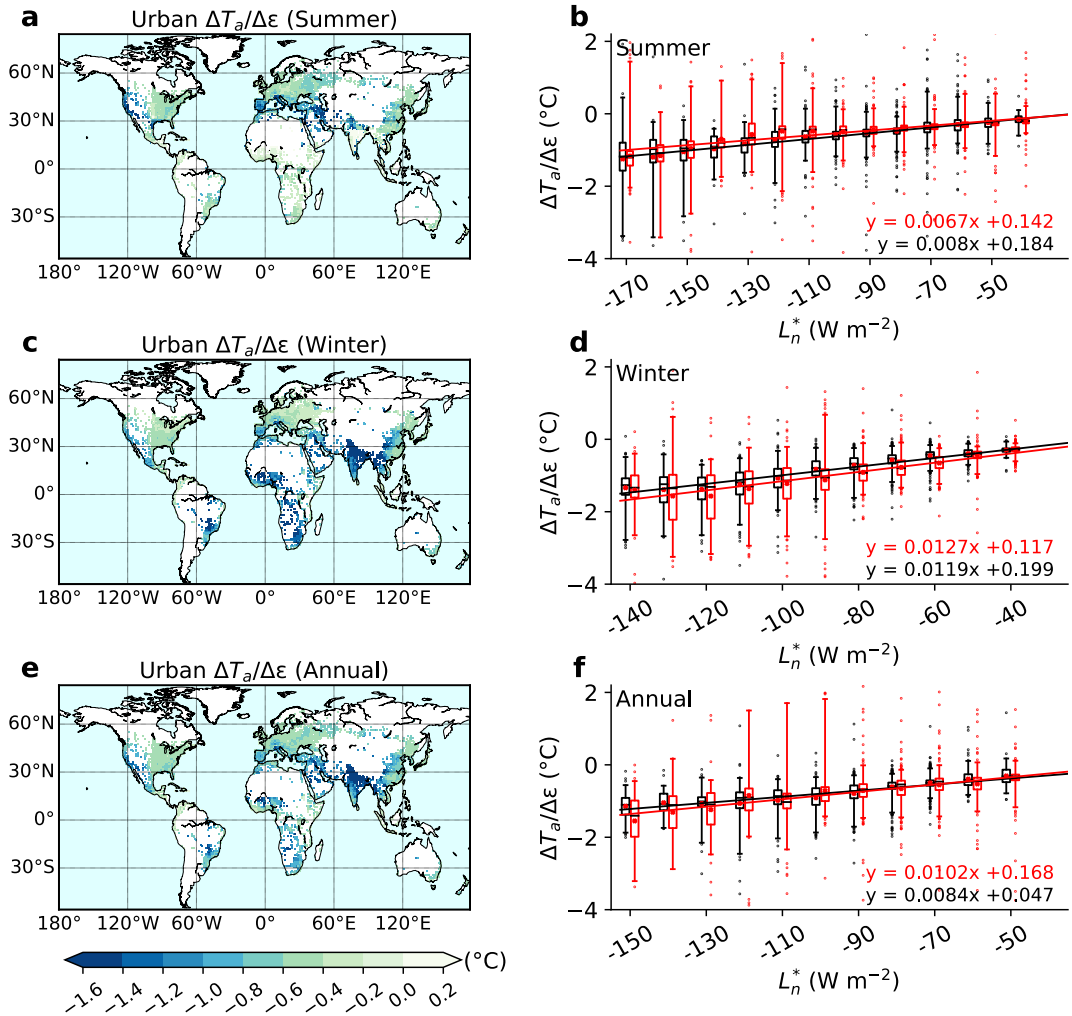

Figure 4. Maps showing urban air temperature sensitivity to urban emissivity (a, c, e) under the current climate, and spatial correlation between this sensitivity and apparent net longwave radiation (b, d, f) under the current (black) and future (red) climates. Data in the right panels are grouped into bins with median (line), 25%–75% range (box), and 2%–98% range (whiskers), and each data point stands for one urban grid. Also shown are linear regression statistics.

As shown in Figure 2 and Equation 3, $\Delta\varepsilon$ influences air temperature via perturbing the net longwave radiation flux. Spatially, a more negative $\Delta T_a/\Delta\varepsilon$ is associated with a more negative "apparent" net longwave radiation (L_n^*; Figures 4a and 4c and S8c, S8d in Supporting Information S1). Here L_n^* is a hypothetical net longwave radiation flux assuming the surface is a black body, which is a concept similar to the apparent net radiation flux proposed in X. Lee (2018). It was calculated as net longwave radiation flux normalized by surface emissivity, expressed as $L_\downarrow - \sigma T_s^4$. We note that L_n^* is a pure climatic variable independent of surface emissivity. A positive linear relationship exists between L_n^* and $\Delta T_a/\Delta\varepsilon$, and this relationship is nearly identical between the current and the future climates (Figures 4b, 4d, and 4f). For the same increase in emissivity, a more negative L_n^* means that the emissivity change produces more cooling. Drier regions with low cloud cover and low air humidity tend to have more negative L_n^* since the downward longwave radiation is reduced, but the upward longwave radiation is enhanced due to high surface temperature.

The temperature sensitivity to albedo ($\Delta T_a/\Delta\alpha$) displays similar spatial patterns to $\Delta T_a/\Delta\varepsilon$ but with larger magnitudes (Figures 4 and 5). An increase in urban albedo leads to more cooling than the same amount of increase in emissivity. Consistent with previous studies (Oleson, Bonan, & Feddema, 2010; Oleson, Bonan, Feddema, Vertenstein, & Kluzek, 2010; Wang et al., 2020), $\Delta T_a/\Delta\alpha$ is negatively correlated with $K_\downarrow$ since albedo change affects shortwave radiation balance (Figures 5 and S8a, S8b in Supporting Information S1). This correlation is

23284277, 2025, 1, Downloaded from https://agupubs.onlinelibrary.wiley.com/doi/10.1029/2024EF005246 by Readcube (Labtiva Inc.), Wiley Online Library on [01/02/2025]. See the Terms and Conditions (https://onlinelibrary.wiley.com/terms-and-conditions) on Wiley Online Library for rules of use; OA articles are governed by the applicable Creative Commons License

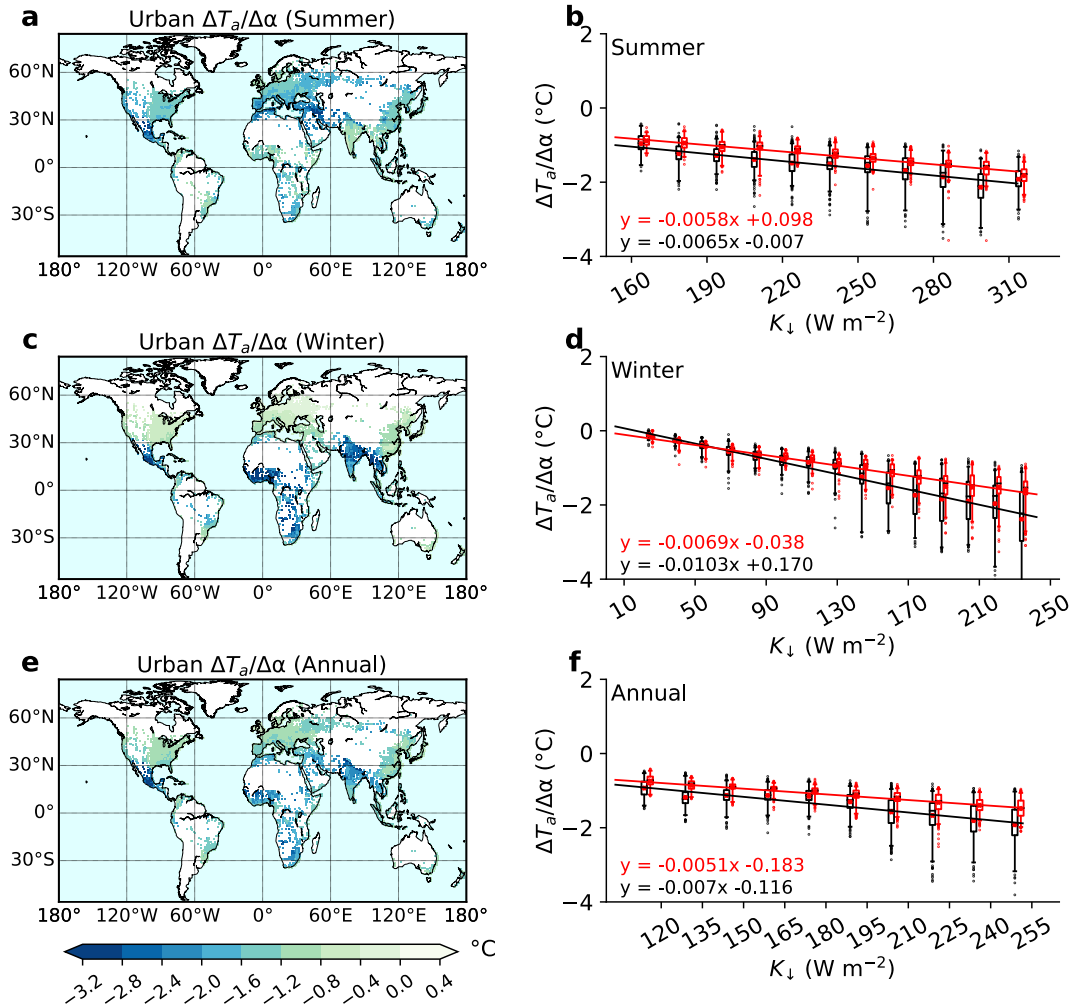

Figure 5. Maps showing urban air temperature sensitivity to urban albedo changes (a, c, e) under the current climate, and spatial correlation of this sensitivity with the incoming solar radiation (b, d, f) under the current (black) and future (red) climates. Data in the right panels are grouped into bins with median (line), 25%–75% range (box), and 2%–98% range (whiskers), and each data point stands for one urban grid.

also linear. While the summer relationship remains relatively stable between the current and the future climate, the future winter $\Delta T_a/\Delta\alpha$ is less sensitive to $K_{\downarrow}$.

3.3. Predicting Air Temperature Responses to Emissivity and Albedo

The strong linear relationships between L_n^* and $\Delta T_a/\Delta\varepsilon$ and between $K_{\downarrow}$ and $\Delta T_a/\Delta\alpha$ enable a parameterization for predicting air temperature changes due to roof material choice. The ΔT_a induced by TAE is predicted using local apparent net longwave radiation and urban surface temperature ($T_{s,u}$), both of which can be obtained for a specific city via satellite or in-situ observations. Firstly, a linear regression is established for $\Delta T_a/\Delta\varepsilon$ and L_n^*:

$$\Delta T_a/\Delta\varepsilon = \beta_1 \times L_n^* + \beta_2 \quad (5)$$

using the DEF2010 and TAE2010 simulations. The regression coefficients β_1 and β_2 are established for the summer, the winter and the full year (Table S1 in Supporting Information S1). Secondly, the urban emissivity change $\Delta\varepsilon$ is calculated with Equation 2. The TAE roof emissivity ε_r is estimated from Equation 1 using hourly $T_{s,u}$ as a proxy for roof surface temperature. The roof snow cover fraction is zero in the summer (Figure S3a in Supporting Information S1), and for the winter and the full year is fitted with a logit function (Figure S9 in Supporting Information S1)

23284277, 2025, 1, Downloaded from https://agupubs.onlinelibrary.wiley.com/doi/10.1029/2024EF005246 by Readcube (Labtiva Inc.), Wiley Online Library on [01/02/2025]. See the Terms and Conditions (https://onlinelibrary.wiley.com/terms-and-conditions) on Wiley Online Library for rules of use; OA articles are governed by the applicable Creative Commons License

10.1029/2024EF005246

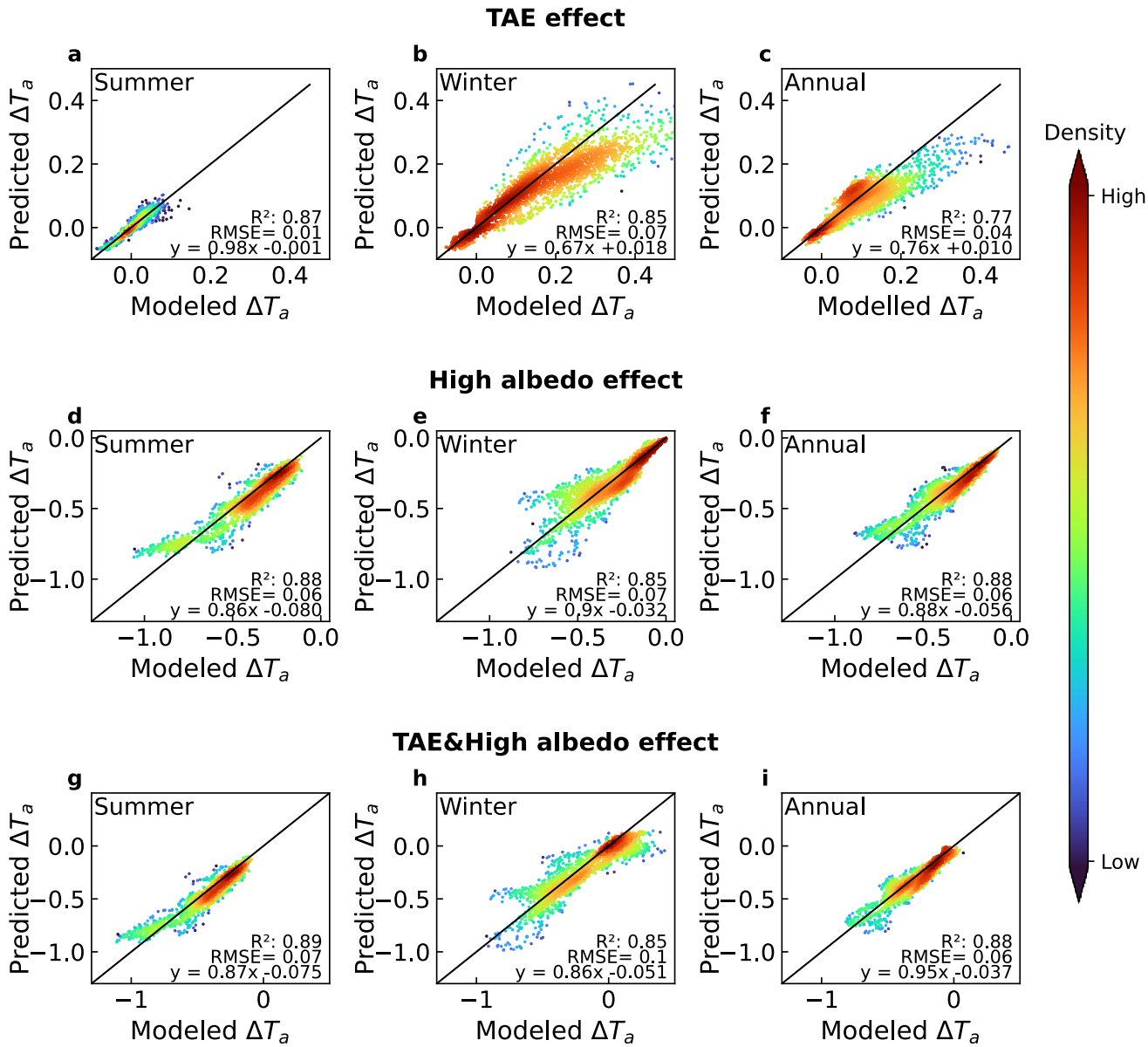

Figure 6. Comparisons between temperature changes (°C) predicted with parameterizations and those from model simulations for future climate. (a–c) Changes caused by temperature-adaptive emissivity (TAE) roofs; (d–f) changes caused by high albedo roofs. (g–i) Changes caused by TAE and high albedo roofs. Each data point represents one grid-cell mean value. Color indicates data density. The black solid line is 1:1. The regression statistics is also shown.

$$f_s = \frac{1}{1 + e^{-k(T_{s,u} - \beta_3)}} \tag{6}$$

where coefficients k and β_3 are determined with regression using the 3-year mean results from DEF2010 (Table S1 in Supporting Information S1). Finally, the air temperature response to TAE is calculated by multiplying $\Delta T_a/\Delta\varepsilon$ from Equation 5 with the estimate of city-scale $\Delta\varepsilon$ from Equation 2.

To demonstrate the predicting power of this parameterization, L_n^* (seasonal or annual mean) and hourly $T_{s,u}$ from DEF2097 are used to predict the air temperature response to TAE under the future scenario. We compare the predicted air temperature changes with the simulated future TAE effect (TAE2097 minus DEF2097; Figures 6a–6c and S10 in Supporting Information S1). The comparison shows good agreement, with high R^2 values (≥0.77)

23284277, 2025, 1, Downloaded from https://agupubs.onlinelibrary.wiley.com/doi/10.1029/2024EF005246 by Readcube (Labtiva Inc.), Wiley Online Library on [01/02/2025]. See the Terms and Conditions (https://onlinelibrary.wiley.com/terms-and-conditions) on Wiley Online Library for rules of use; OA articles are governed by the applicable Creative Commons License

23284277, 2025, 1, Downloaded from https://agupubs.onlinelibrary.wiley.com/doi/10.1029/2024EF005246 by Readcube (Labtiva Inc.), Wiley Online Library on [01/02/2025]. See the Terms and Conditions (https://onlinelibrary.wiley.com/terms-and-conditions) on Wiley Online Library for rules of use; OA articles are governed by the applicable Creative Commons License

and low root mean square error (RMSE) values of 0.01, 0.07, and 0.04°C for summer, winter, and annual results, respectively. This simple parameterization can predict future ΔT_a induced by TAE with good accuracy.

Similarly, we propose another parameterization to predict air temperature response to albedo change. The city-scale change in albedo ($\Delta\alpha$) is calculated from the difference between fixed high albedo (0.75) and default roof α_d, scaled by $1-f_s$ and f_r (Equation 4). A linear regression between $\Delta T_a/\Delta\alpha$ and $K_\downarrow$ is developed on the basis of current climate simulations as

$$\Delta T_a/\Delta\alpha = \beta_4 \times K_\downarrow + \beta_5 \quad (7)$$

Here the ΔT_a is the air temperature difference between TAE&high albedo2010 and TAE2010. The regression coefficients β_4 and β_5 are given in Table S1 in Supporting Information S1 for summer, winter, and annual results. The air temperature change induced by albedo increase is the product of $\Delta T_a/\Delta\alpha$ from Equation 7 and the estimate of $\Delta\alpha$ from Equation 4. This parameterization result for the future climate shows very good agreement with the modeled ΔT_a (TAE&high albedo 2097 minus TAE2097), with $R^2 \geq 0.85$ and the RMSE smaller than 0.08°C (Figures 6d–6f and S11 in Supporting Information S1). Although the future $\Delta T_a/\Delta\alpha$ versus $K_\downarrow$ differs slightly from that for the current climate (Figure 5), these differences do not significantly compromise the predicting power of this parametrization.

The combined effect of TAE and high albedo is calculated as the sum of the air temperature responses to TAE and to high albedo (Figures 6g–6i). The predicted ΔT_a induced by TAE and high albedo shows good agreement with the simulated air temperature changes (TAE&high albedo 2097 minus DEF2097), with $R^2 \geq 0.85$ and the RMSE of 0.06 to 0.1°C.

The above parameterization scheme assumes that the urban surface temperature $T_{s,u}$ is known. In situations where data on $T_{s,u}$ is not available, the grid mean air temperature can be used in its place, with similar performance. For example, the R^2 and RMSE for the annual ΔT_a due to TAE and high albedo remain the same if the grid mean temperature is used as an input variable. This parameterization can estimate air temperature response to any combinations of roof emissivity and albedo, allowing first-order evaluation of different roof materials.

3.4. Responses of Building Energy Demand for Space Heating and Cooling

High albedo roofs cause winter heating energy penalty. Here, we examine the primary building energy demand for space heating and cooling per unit urban area (Q_e, W m^{-2}). Under current climate, albedo cooling decreases summer Q_e by 0 to 1.3 W m^{-2} except for Northern North America (Figure 7a and Table S2 in Supporting Information S1; the summer Q_e increase in Northern North America due to albedo effect is discussed in Text S2 in Supporting Information S1.) In the winter, high albedo increases Q_e by up to 1.0 W m^{-2}, with a larger heating energy penalty in mid-latitude regions, such as Central Asia, the Mediterranean Coast, East Asia, Australia, and the Southern North America (Figure 7b and Table S2 in Supporting Information S1). These regions experience relatively cold winters, and the local temperature is sensitive to albedo changes (Figure 5c). As an example, for Los Angeles (34.1°N, 118.2°W), a densely populated mid-latitude city, high roof albedo increases the winter Q_e by 8% (1.3 W m^{-2}). High albedo still reduces winter energy use in tropical regions, including Southeast Asia, North Africa, and Amazon Basin, where cities experience warm temperatures all year around. In high-latitude regions (e.g., North Asia) where winter air temperature is insensitive to albedo changes, the changes in energy use are negligible.

Annually, the increased heating load due to high albedo exceeds the reduced cooling demand in temperate and boreal regions (Figure 8a and Table S3 in Supporting Information S1), with total energy use (E) increases by 2.5% and 1.7% (38.1 and 60.1 GW), respectively, after high albedo roofs are adopted (Figure 8 and Table S3 in Supporting Information S1). Tropical cities benefit from albedo cooling, with E decreased by 20.8% (22.2 GW). High albedo roofs reduce the building energy use of arid cities slightly by 0.7% (3.1 GW).

The winter heating energy penalty of high roof albedo is largely mitigated by TAE. In the summer, TAE roofs have negligible influence on energy use due to the small air temperature response to TAE (Figures 1c and 7a). In the winter, TAE roofs provide warming and thus decrease energy use for space heating, particularly in mid-latitude regions with cold winters. The annual Q_e reduction because of TAE roofs is evident in Central Asia, the Mediterranean Coast, East Asia, Australia, the Southern North America, Europe, Northern North America,

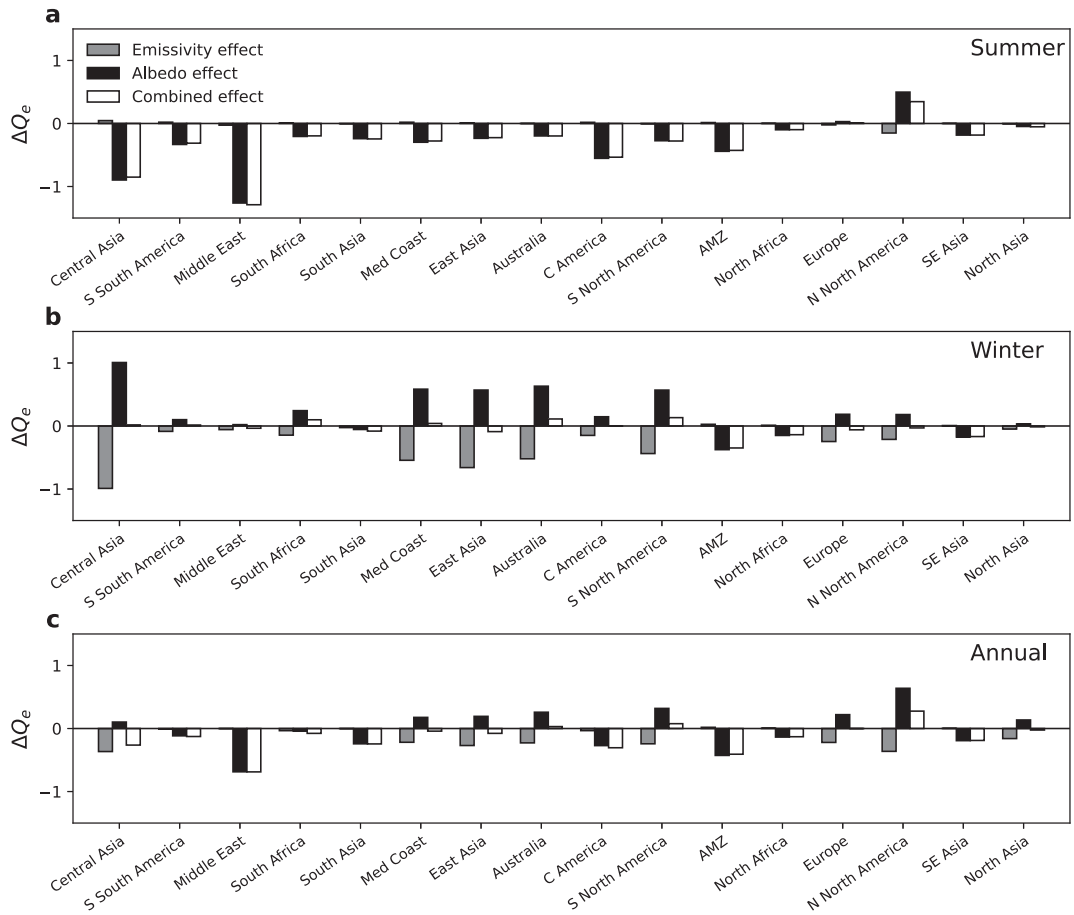

Figure 7. Regional changes in building energy demand per urban area (W m^{-2}) under the current climate. Region definitions and geographic boundaries are given in Figure S3 in Supporting Information S1.

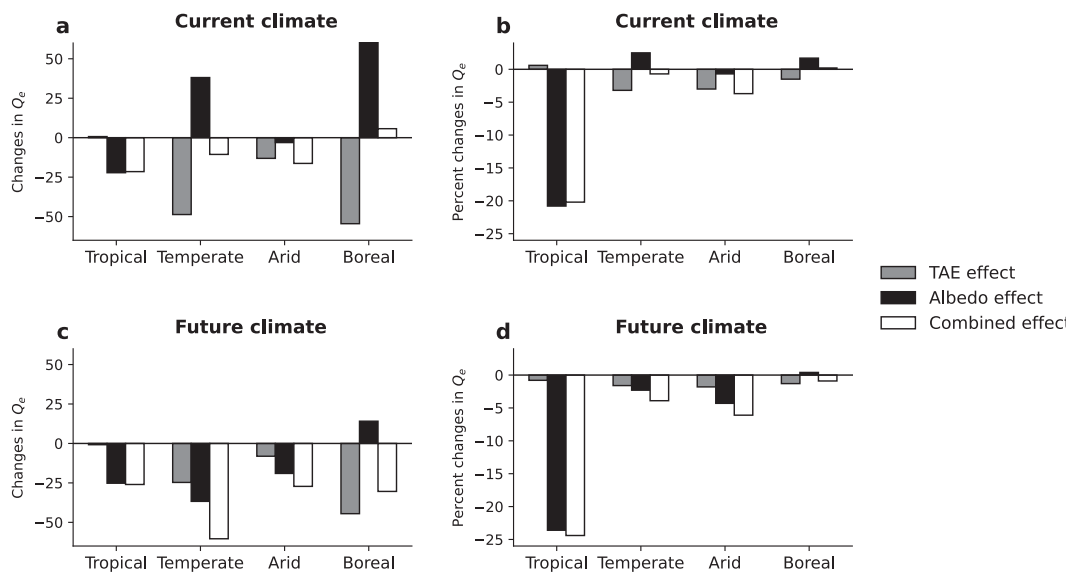

Figure 8. Changes in regional building energy demand (Q_e) in total power (GW) and percent change (%) induced by temperature-adaptive emissivity, high albedo, and their combined effects under the current and future climate. The climate regions are divided by the Köppen-Geiger climate classification (Rubel & Kottek, 2010). The percentage changes are calculated with respect to the total building energy demand of that region from DEF2010.

23284277, 2025, 1, Downloaded from https://agupubs.onlinelibrary.wiley.com/doi/10.1029/2024EF005246 by Readcube (Labtiva Inc.), Wiley Online Library on [01/02/2025]. See the Terms and Conditions (https://onlinelibrary.wiley.com/terms-and-conditions) on Wiley Online Library for rules of use; OA articles are governed by the applicable Creative Commons License

23284277, 2025, 1, Downloaded from https://agupubs.onlinelibrary.wiley.com/doi/10.1029/2024EF005246 by Readcube (Labtiva Inc.), Wiley Online Library on [01/02/2025]. See the Terms and Conditions (https://onlinelibrary.wiley.com/terms-and-conditions) on Wiley Online Library for rules of use; OA articles are governed by the applicable Creative Commons License

and North Asia, ranging from 0.16 W m^{-2} (North Asia) to 0.36 W m^{-2} (Central Asia). When high albedo and TAE are both adopted, annual Q_e decreases or changes little (<+0.08 W m^{-2}) in most regions except for Northern North America (+0.27 W m^{-2}; Figure 7c and Table S2 in Supporting Information S1). In cold seasons, the TAE warming offset albedo cooling, mitigating the winter heating energy penalty effectively. Overall, roofs with TAE and high albedo change the annual E little in the boreal climate region, and decrease the annual E by 20.2%, 0.7%, and 3.7% in tropical, temperate, and arid climate regions, respectively (Figures 8a and 8b and Table S3 in Supporting Information S1). TAE contributes to urban energy sustainability by offsetting heating energy penalty in the winter.

The impacts of TAE roofs on building energy demand are subject to change under global warming. The heating energy penalty of albedo effect in temperate and boreal regions disappears or becomes smaller in a warmer climate (Figure 8 and Table S3 in Supporting Information S1). High albedo reduces the future E by a greater amount of 25.2 and 19.0 GW for tropical and arid regions, respectively than in current climate. The impact of TAE on E generally becomes smaller in the future because of two reasons. First, the winter TAE warming is weaker in a warmer background climate (Figure S7b in Supporting Information S1). Second, future building heating load is also reduced. During 2097 to 2099, high albedo combined with TAE provides net energy saving for all climate zones (Figure 8 and Table S3 in Supporting Information S1).

4. Discussion

4.1. Practical Implications on Climate-Specific Roof Material Choices

Our results provide guidance on roof material choices for cities across diverse background climates. Mid-latitude cities in temperate and arid climates such as cities in Central Asia, Southern South America, Middle East, Mediterranean Coast, and Australia benefit the most from roofs with simultaneous TAE and high albedo. These roofs can mitigate hot and cold extremes, create summer cooling and avoid heating energy penalty in the winter (Figures 1e and 1f and 7c and Table S2 in Supporting Information S1). However, TAE is neither necessary nor effective for tropical cities in regions such as South Asia, Central America, and Amazon basin, which require cooling throughout the year. These cities benefit the most from conventional radiative cooling materials or other super cool materials that provide constant cooling, reducing temperature and building energy use. For cities north of 50°N (i.e., North Asia and Northern North America), neither TAE nor high albedo roofs significantly impact winter air temperature because of high snow cover (Figure S3b in Supporting Information S1) and low climate sensitivity to emissivity and albedo (Figures 4c and 5c). Other innovative strategies are required to mitigate cold and hot extremes for these cities. Besides, the optimal emissivity and albedo may vary for different cities. This study uses a moderately high albedo of 0.75. Having albedo higher than 0.75 provides more cooling all year around, which benefits tropical cities (Figure 5).

The snow effect should be considered when choosing climate-specific roof materials because snow cover plays an important role in shaping radiative mitigation strategies. In cities north of 45°N, the fraction of roof area covered by snow in the winter ($f_{s,r}$) is 0.62 ± 0.35 (mean ± one standard deviation). Because the TAE coating is largely masked by snow, TAE produces little winter warming and energy saving for these cities under the current climate. With future warming under the SSP5-8.5 scenario, the snow effect is only evident in Siberia, North Europe, and Northern North America. The average $f_{s,r}$ is 0.2 for cities north of 45°N, and the benefit of TAE becomes larger.

4.2. Climate Sensitivity to TAE Transition Temperatures

At the same local temperature, the transition temperatures control whether the TAE roof is in the low-emissivity or high-emissivity state, which can be adjusted by changing the chemical composition of the TAE coating (S. Lee et al., 2021). Tang et al. (2020) present a technique to program the two temperature thresholds T_1 and T_2. It is possible to fine-tune these thresholds according to local climate conditions to maximize the TAE climate benefits. At a lower T_1, the TAE roof will be in the low-emissivity state for shorter durations. Conversely, at a lower T_2, the TAE roof will be in the high-emissivity state for a longer duration. A reduction in T_1 or T_2 leads to higher overall emissivity and causes more cooling. The TAE effect shown in Figures 6a–6c is based on the default T_1 and T_2 of 19 and 27°C, respectively (Tang et al., 2021). Here, we investigate the sensitivity of the TAE effect to T_1 and T_2 (Equations 1 and 2). This is done with the parameterization scheme described in Section 3.3 and aided by modeled urban surface temperature (at hourly time steps), modeled air temperature sensitivity to emissivity, and roof snow

10.1029/2024EF005246

23284277, 2025, 1, Downloaded from https://agupubs.onlinelibrary.wiley.com/doi/10.1029/2024EF005246 by Readcube (Labtiva Inc.), Wiley Online Library on [01/02/2025]. See the Terms and Conditions (https://onlinelibrary.wiley.com/terms-and-conditions) on Wiley Online Library for rules of use; OA articles are governed by the applicable Creative Commons License

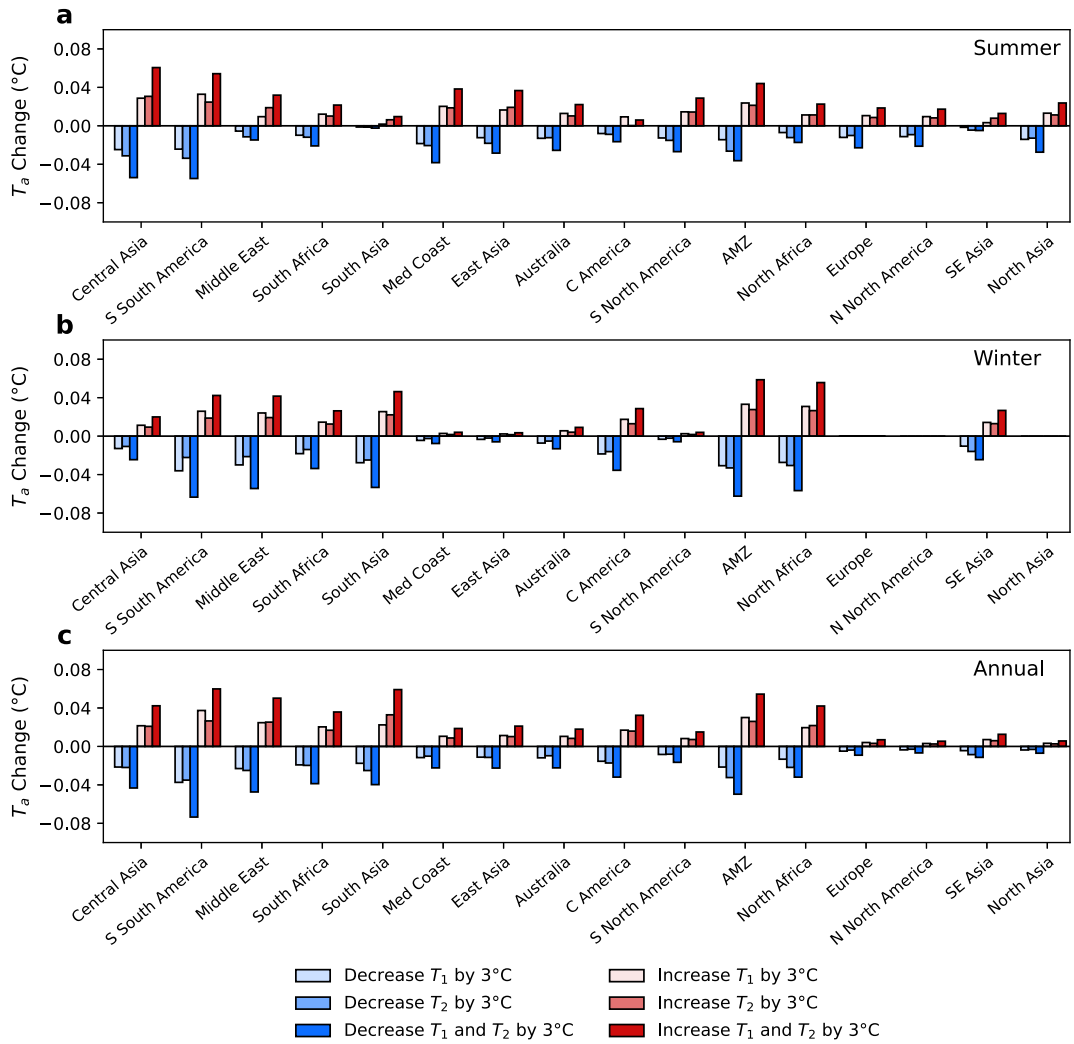

Figure 9. Sensitivity of air temperature to the temperature-adaptive emissivity temperature thresholds under the current climate. Region definitions and geographic boundaries are given in Figure S3 in Supporting Information S1.

fraction. Figure 9 shows the results for six T_1 and T_2 combinations. The reference state in this case is the TAE with $T_1 = 19$°C and $T_2 = 27$°C. A negative temperature change means more cooling than this reference state.

First, reducing T_1 and T_2 by 3°C is beneficial for many mid- and low-latitude regions (Figure 9). For Middle East, South Asia, Central America, Amazon Basin, North Africa, and Southeast Asia with warm winter and hot summer, reducing T_1 and T_2 provides additional summer cooling by 0 to 0.04°C and lowers the winter temperature by 0.02 to 0.06°C relative to the TAE baseline. As for Mediterranean Coast, East Asia, Australia, and the Southern North America with a hot summer and cold winter, they experience an additional 0.03 to 0.04°C summer cooling and negligible change in winter temperature after reducing T_1 and T_2 by 3°C. For example, in Beijing (39.9° N, 116.4° E), the parameterization predicts the current summer and winter ΔT_a induced by default TAE roofs to be +0.05°C and +0.26°C with default T_1 and T_2. When the T_1 and T_2 are reduced by 3°C, the summer and winter ΔT_a induced by TAE become +0.008°C and +0.26°C, respectively, providing less undesired summer warming without compromising the desired winter warming. Second, increasing T_1 and T_2 leads to more TAE warming in both the summer and the winter (Figure 9). In regions where winter warming is desired and summer heat stress is not a concern, it may be advantageous to adjust these two thresholds upward. Third, changing T_1 or T_2 by the same amount yields similar temperature changes. Increasing both T_1 and T_2 simultaneously by the same amount produces temperature changes that are roughly equal to the sum of the changes from increasing T_1 and T_2 separately.

23284277, 2025, 1, Downloaded from https://agupubs.onlinelibrary.wiley.com/doi/10.1029/2024EF005246 by Readcube (Labtiva Inc.), Wiley Online Library on [01/02/2025]. See the Terms and Conditions (https://onlinelibrary.wiley.com/terms-and-conditions) on Wiley Online Library for rules of use; OA articles are governed by the applicable Creative Commons License

Besides adjusting T_1 and T_2 thresholds, our parameterization scheme can be used to evaluate the sensitivity to the lowest and highest emissivity of this material as well as its albedo, aiding optimization of roof material choice for specific cities.

4.3. Limitations

The original TAE cooling surface developed by Tang et al. (2021) exhibits emissivity behaviors in the sky window (wavelength 8–13 μm). However, CTSM uses broadband emissivity for surface energy balance computation, where the same emissivity value is assigned to all infrared wavelengths. The difference between broadband and sky-window emitters depends on ambient temperature and local climate conditions. Studies have shown that an ideal broadband emitter provides more cooling than an ideal sky-window emitter when the surface temperature is above or close to ambient air temperature (Z. Huang & Ruan, 2017; Yin et al., 2020). A theoretical calculation shows that their difference in net cooling power is less than 15 W m^{-2} when the temperature difference between surface and ambient air is within 10°C (D. Zhao et al., 2019), which is about 8% of the absolute net cooling power produced by broadband (185 W m^{-2}) and sky-window emitters (200 W m^{-2}). In humid climate with strong downward longwave radiation, broadband emitters have lower cooling power than sky-window emitters because they absorb more downward longwave radiation (Feng et al., 2020). These past studies consider ideal sky-window emitters with emissivity of 1 in the sky window and zero in other infrared wavelengths. However, we note that the TAE cooling surface is not a perfect sky-window emitter since the emissivity outside the sky window is non-zero. Tang et al. (2021) reported that the TAE cooling material and a broadband emitter with the same emissivity offer similar net cooling power, with the deviation smaller than 10% even when the temperature difference between the surface and ambient air exceeds 20°C. Therefore, using a broadband emissivity in CTSM is a reasonable approximation for performance evaluation of the original TAE material.

Another limitation of this study is that the emissivity at high temperatures used in our simulations (0.98) is higher than the value of 0.9 reported by Tang et al., 2021. We note that some PRC surfaces (C. Wang et al., 2024) and other TAE materials (C. Chen et al., 2024; Xie et al., 2024) can achieve emissivity greater than 0.96. According to the parameterization we described in Section 3.3, by changing the TAE emissivity in the high-emissivity state from 0.98 to 0.90, the summer temperature change is 0.02 ± 0.01°C (mean of regional values ±1 standard deviation of the 16 regions shown in Figure S3 in Supporting Information S1, under the current climate), which will not impact our conclusions qualitatively.

In our simulations, we used prescribed atmospheric conditions to force the CTSM calculations, assuming implicitly that TAE and high albedo roofs have no influence on the atmosphere above. This assumption is valid if the surface radiative property change occurs in a small scale (Chen & Dirmeyer, 2020). However, large-scale adoption of these roofs may alter atmospheric conditions and trigger land-atmospheric feedback. In a numerical experiment on idealized land surface with varied albedo anomalies, land brightening triggers mesoscale circulation and increases regional precipitation. The enhanced evaporation further strengthens the cooling initiated by albedo increase (Cheng et al., 2023). In a modeling study on the climate effect of super cool material, an inversion layer develops over a land surface with high albedo, a consequence of which is a reduction of near-surface wind (Khan et al., 2021). Weaker wind in the boundary layer causes reduction of moisture vertical transport and hinders cloud formation (Mohammed et al., 2021), which in turn will increase the incoming solar radiation and counteract the albedo cooling effect. On the other hand, reduction in cloud contributes to a more negative net apparent longwave radiation, and we expect a greater temperature reduction for the same amount of emissivity increase (Figure 4). To what extent these feedback processes matter likely depends on local soil moisture status and regional circulation patterns. New progress can be made with fine-resolution simulations that allow the surface and the atmosphere to interact with each other.

Large-scale application of TAE materials faces several challenges. Currently. there is no price estimation for the TAE material, but its production cost is expected to be much higher than existing commercial cool roofs (USD 8 to 65 per m^2) and green roofs (initial cost at USD 108 to 270 per m^2; Santamouris et al., 2011; Tang et al., 2021; US EPA, 2008). Currently, temperature-adaptive radiative coatings cannot be customized for color, but aesthetic considerations are crucial for commercializing these novel materials. Potential solutions to producing colored radiative cooling material could be based on photoluminescence (Min et al., 2022) or selective absorption (Yalçın et al., 2020). Finally, information on TAE material durability is needed to provide a comprehensive price evaluation.

23284277, 2025, 1, Downloaded from https://agupubs.onlinelibrary.wiley.com/doi/10.1029/2024EF005246 by Readcube (Labtiva Inc.), Wiley Online Library on [01/02/2025]. See the Terms and Conditions (https://onlinelibrary.wiley.com/terms-and-conditions) on Wiley Online Library for rules of use; OA articles are governed by the applicable Creative Commons License

5. Conclusions

In this study, we assess the climate and energy benefits of a novel roof coating with TAE and high albedo using a global climate model. Three sets of factorial experiments are carried out to separate the effects of TAE and high albedo and their combined effect.

We find that roofs with TAE have a negligible effect on air temperature under hot conditions, such as summer season at mid-to high latitudes and all seasons near the equator. However, they provide winter warming in extratropical cities by up to 0.54°C (99th percentile). Conversely, high albedo alone reduces winter temperature and leads to non-negligible winter heating energy penalty for regions with cold winters, resulting in a 2.5% (38.1 GW) and 1.7% (60.2 GW) increase in total energy demand for space heating and cooling in temperate and boreal climates. The adoption of roofs with TAE and high albedo enhances both thermal comfort and urban sustainability, especially in mid latitudes. It reduces summer daily maximum temperature and increases winter daily minimum temperatures, changing the annual building energy demand by −20.2%, −0.7%, −3.7%, and +0.2% in tropical, temperate, arid, and boreal climate zones.

The use of high albedo roofs reduces summer temperature at mid-to high latitudes and all-season temperature near the equator. In the winter, the TAE warming in mid-latitude cities can fully offset the undesired winter cooling induced by high albedo. In summary, tropical, low latitude cities benefit from conventional radiative cooling material with constant cooling effect. The combination of TAE and high albedo suits mid-latitude cities with evident seasonality. However, radiative mitigation strategies generally are not influential in winter for boreal, high latitude cities. Other innovative strategies are needed to achieve thermal regulation and heating energy saving.

There are positive linear relationships between air temperature sensitivity to emissivity ($\Delta T_a/\Delta\varepsilon$) and local apparent net longwave radiation and negative linear relationships between air temperature sensitivity to albedo ($\Delta T_a/\Delta\alpha$) and incoming solar radiation. Utilizing these relationships, we have developed a simple parameterization to predict air temperature response to roof emissivity and albedo. This parameterization offers first order evaluations of climate responses to different roofing materials.

Data Availability Statement

The Community Terrestrial Systems Model is available at https://github.com/ESCOMP/CTSM. The data and Python code used to produce the figures in this paper are available on Figshare (https://doi.org/10.6084/m9.figshare.26264063.v1; K. Zhang et al., 2024).

Acknowledgments
XL and LZ acknowledge support by the US National Science Foundation (Grants 1933630 and 2145362), LZ acknowledges support by the Institute for Sustainability, Energy and Environment at the University of Illinois Urbana-Champaign. KZ acknowledges support by a Yale Graduate Fellowship and the HMEI Environmental Fellows Program at Princeton University. Contributions from KO are based upon work supported by the NSF National Center for Atmospheric Research, which is a major facility sponsored by the U.S. National Science Foundation under Cooperative Agreement No. 1852977. High-performance computing support from Derecho (https://doi.org/10.5065/qx9a-pg09) was provided by NCAR's Computational and Information Systems Laboratory, sponsored by the US National Science Foundation.

References

Bonan, G. (1996). A land surface model (LSM version 1.0) for ecological, hydrological, and atmospheric studies: Technical description and user's guide. NCAR/TN-417+STR NCAR Technical Note. National Center for Atmospheric Research, Boulder, CO. https://doi.org/10.5065/D6DF6P5X

Cabeza, L. F., Bai, Q., Bertoldi, P., Kihila, J. M., Lucena, A. F. P., Mata, É., et al. (2022). 2022: Buildings. In *IPCC, 2022: Climate change 2022: Mitigation of climate change. Contribution of working group III to the sixth assessment report of the intergovernmental panel on climate change*. Cambridge University Press. https://doi.org/10.1017/9781009157926.011

Chen, C., Xia, X., Hu, J., Song, R., Li, B., Hu, H., et al. (2024). Zero-energy switchable radiative cooler for enhanced building energy efficiency. *Journal of Photonics for Energy*, *14*(02), 1–20. https://doi.org/10.1117/1.jpe.14.028501

Chen, L., & Dirmeyer, P. A. (2020). Reconciling the disagreement between observed and simulated temperature responses to deforestation. *Nature Communications*, *11*(1), 1–10. https://doi.org/10.1038/s41467-019-14017-0

Cheng, Y., Hu, Z., & Mccoll, K. A. (2023). Anomalously darker land surfaces become wetter due to mesoscale circulations. *Geophysical Research Letters*, *50*(17), 1–10. https://doi.org/10.1029/2023GL104137

Danabasoglu, G., Lamarque, J. F., Bacmeister, J., Bailey, D. A., DuVivier, A. K., Edwards, J., et al. (2020). The Community Earth System Model Version 2 (CESM2). *Journal of Advances in Modeling Earth Systems*, *12*(2), 1–35. https://doi.org/10.1029/2019MS001916

Feng, J., Gao, K., Santamouris, M., Wei, K., & Ranzi, G. (2020). Dynamic impact of climate on the performance of daytime radiative cooling materials. *Solar Energy Materials and Solar Cells*, *208*, 110426. https://doi.org/10.1016/j.solmat.2020.110426

Feng, J., Saliari, M., Gao, K., & Santamouris, M. (2022). On the cooling energy conservation potential of super cool roofs. *Energy and Buildings*, *264*, 112076. https://doi.org/10.1016/j.enbuild.2022.112076

Gao, J., & O'Neill, B. C. (2020). Mapping global urban land for the 21st century with data-driven simulations and Shared Socioeconomic Pathways. *Nature Communications*, *11*(1), 1–12. https://doi.org/10.1038/s41467-020-15788-7

Huang, X., Bou-Zeid, E., Pigliautile, I., Pisello, A. L., & Mandal, J. (2024). Optimizing retro-reflective surfaces to untrap radiation and cool cities. *Nature Cities*, *1*(4), 275–285. https://doi.org/10.1038/s44284-024-00047-3

Huang, Z., & Ruan, X. (2017). Transfer Nanoparticle embedded double-layer coating for daytime radiative cooling. *International Journal of Heat and Mass Transfer*, *104*, 890–896. https://doi.org/10.1016/j.ijheatmasstransfer.2016.08.009

IEA. (2019). Global status report for buildings and construction. Retrieved from https://www.iea.org/reports/global-status-report-for-buildings-and-construction-2019

Isaac, M., & Vuuren, D. P. V. (2009). Modeling global residential sector energy demand for heating and air conditioning in the context of climate change. *Energy Policy*, *37*(2), 507–521. https://doi.org/10.1016/j.enpol.2008.09.051

Jackson, T. L., Feddema, J. J., Oleson, K. W., Bonan, G. B., & Bauer, J. T. (2010). Parameterization of urban characteristics for global climate modeling. *Annals of the Association of American Geographers*, *100*(4), 848–865. https://doi.org/10.1080/00045608.2010.497328

Khan, A., Carlosena, L., Khorat, S., Khatun, R., Doan, Q., Feng, J., & Santamouris, M. (2021). On the winter overcooling penalty of super cool photonic materials in cities. *Solar Energy Advances*, *1*, 100009. https://doi.org/10.1016/j.seja.2021.100009

Lawrence, D., Fisher, R., Koven, C., Oleson, K., Swenson, S., & Vertenstein, M. (2018). Technical description of version 5.0 of the community land model (CLM). NCAR/TN-478+STR NCAR Technical Note. National Center for Atmospheric Research.

Lawrence, D. M., Fisher, R. A., Koven, C. D., Oleson, K. W., Swenson, S. C., Bonan, G., et al. (2019). The community land model version 5: Description of new features, benchmarking, and impact of forcing uncertainty. *Journal of Advances in Modeling Earth Systems*, *11*(12), 4245–4287. https://doi.org/10.1029/2018MS001583

Lee, S., Hippalgaonkar, K., Yang, F., Hong, J., Ko, C., Suh, J., et al. (2021). Anomalously low electronic thermal conductivity in metallic vanadium dioxide. *Science*, *355*(6323), 371–374. https://doi.org/10.1126/science.aag0410

Lee, X. (2018). *Fundamentals of boundary- layer meteorology*. Springer. https://doi.org/10.1007/978-3-319-60853-2

Li, X. "C"., Zhao, L., Oleson, K., Zhou, Y., Qin, Y., Zhang, K., & Fang, B. (2024). Enhancing urban climate-energy modeling in the community Earth system model (CESM) through explicit representation of urban air-conditioning adoption. *Journal of Advances in Modeling Earth Systems*, *16*(4). https://doi.org/10.1029/2023MS004107

Lipson, M., Grimmond, S., Best, M., Abramowitz, G., Coutts, A., Tapper, N., et al. (2023). Evaluation of 30 urban land surface models in the Urban-PLUMBER project: Phase 1 results. *Quarterly Journal of the Royal Meteorological Society*, *150*(758), 126–169. https://doi.org/10.1002/qj.4589

Min, S., Jeon, S., Yun, K., & Shin, J. (2022). All-color sub-ambient radiative cooling based on photoluminescence. *ACS Photonics*, *9*(4), 1196–1205. https://doi.org/10.1021/acsphotonics.1c01648

Mohammed, A., Khan, A., & Santamouris, M. (2021). On the mitigation potential and climatic impact of modified urban albedo on a subtropical desert city. *Building and Environment*, *206*, 108276. https://doi.org/10.1016/j.buildenv.2021.108276

Oleson, K. W., Bonan, G. B., & Feddema, J. (2010). Effects of white roofs on urban temperature in a global climate model. *Geophysical Research Letters*, *37*(3), 1–7. https://doi.org/10.1029/2009GL042194

Oleson, K. W., Bonan, G. B., Feddema, J. J., Vertenstein, M., & Kluzek, E. (2010). Technical description of an urban parameterization for the community land model (CLMU) (No. NCAR/TN-480+STR). *NCAR Technical Note*. https://doi.org/10.5065/D6K35RM9

Oleson, K. W., & Feddema, J. (2020). Parameterization and surface data improvements and new capabilities for the community land model urban (CLMU). *Journal of Advances in Modeling Earth Systems*, *12*(2), 1–30. https://doi.org/10.1029/2018MS001586

Rubel, F., & Kottek, M. (2010). Observed and projected climate shifts 1901-2100 depicted by world maps of the Köppen-Geiger climate classification. *Meteorologische Zeitschrift*, *19*(2), 135–141. https://doi.org/10.1127/0941-2948/2010/0430

Santamouris, M. (2014). Cooling the cities – A review of reflective and green roof mitigation technologies to fight heat island and improve comfort in urban environments. *Solar Energy*, *103*, 682–703. https://doi.org/10.1016/j.solener.2012.07.003

Santamouris, M., Synnefa, A., & Karlessi, T. (2011). Using advanced cool materials in the urban built environment to mitigate heat islands and improve thermal comfort conditions. *Solar Energy*, *85*(12), 3085–3102. https://doi.org/10.1016/j.solener.2010.12.023

Santamouris, M., & Yun, G. Y. (2020). Recent development and research priorities on cool and super cool materials to mitigate urban heat island. *Renewable Energy*, *161*, 792–807. https://doi.org/10.1016/j.renene.2020.07.109

Shen, H., Tan, H., & Tzempelikos, A. (2011). The effect of reflective coatings on building surface temperatures, indoor environment and energy consumption—An experimental study. *Energy and Buildings*, *43*(2–3), 573–580. https://doi.org/10.1016/j.enbuild.2010.10.024

Sinsel, T., Simon, H., Broadbent, A. M., Bruse, M., & Heusinger, J. (2021). Modeling impacts of super cool roofs on air temperature at pedestrian level in mesoscale and microscale climate models. *Urban Climate*, *40*, 101001. https://doi.org/10.1016/j.uclim.2021.101001

Sudmanns, M., Tiede, D., Augustin, H., & Lang, S. (2020). Assessing global Sentinel-2 coverage dynamics and data availability for operational Earth observation (EO) applications using the EO-Compass. *International Journal of Digital Earth*, *13*(7), 768–784. https://doi.org/10.1080/17538947.2019.1572799

Synnefa, A., Santamouris, M., & Akbari, H. (2007). Estimating the effect of using cool coatings on energy loads and thermal comfort in residential buildings in various climatic conditions. *Energy and Buildings*, *39*(11), 1167–1174. https://doi.org/10.1016/j.enbuild.2007.01.004

Tan, H., Kotamarthi, R., Wang, J., Qian, Y., & Chakraborty, T. C. (2023). Impact of different roofing mitigation strategies on near-surface temperature and energy consumption over the Chicago metropolitan area during a heatwave event. *Science of the Total Environment*, *860*, 160508. https://doi.org/10.1016/j.scitotenv.2022.160508

Tang, K., Dong, K., Li, J., Gordon, M. P., Reichertz, F. G., Urban, J. J., et al. (2021). Temperature-adaptive radiative coating for all-season household thermal regulation. *Science*, *1509*(6574), 1504–1509. https://doi.org/10.1126/science.abf7136

Tang, K., Wang, X., Dong, K., Li, Y., Li, J., Sun, B., et al. (2020). A thermal radiation modulation platform by emissivity engineering with graded metal–insulator transition. *Advanced Materials*, *32*(36), 1–6. https://doi.org/10.1002/adma.201907071

US EPA. (2008). Reducing urban heat islands: Compendium of strategies. Retrieved from https://www.epa.gov/heatislands/heat-island-compendium

Wang, C., Chen, H., & Wang, F. (2024). Passive daytime radiative cooling materials toward real-world applications. *Progress in Materials Science*, *144*, 101276. https://doi.org/10.1016/j.pmatsci.2024.101276

Wang, L., Huang, M., & Li, D. (2020). Where are white roofs more effective in cooling the surface? *Geophysical Research Letters*, *47*(15), 1–11. https://doi.org/10.1029/2020GL087853

Wang, P., Zhang, W., Liu, J., He, P., Wang, J., Huang, L., & Zhang, B. (2023). Analysis and intervention of heatwave related economic loss: Comprehensive insights from supply, demand, and public expenditure into the relationship between the influencing factors. *Journal of Environmental Management*, *326*, 116654. https://doi.org/10.1016/j.jenvman.2022.116654

Xie, H., Yin, H., & Fan, C. (2024). Realization of an adaptive radiative cooler with a multilayer-filter VO2-based Fabry-Pérot cavity. *Chinese Physics Letters*, *41*(4), 044202. https://doi.org/10.1088/0256-307X/41/4/044202

Yalçın, R. A., Blandre, E., Joulain, K., & Drévillon, J. (2020). Colored radiative cooling coatings with nanoparticles. *ACS Photonics*, *7*(5), 1312–1322. https://doi.org/10.1021/acsphotonics.0c00513

Yin, X., Yang, R., Tan, G., & Fan, S. (2020). Terrestrial radiative cooling: Using the cold universe as a renewable and sustainable energy source. *Science*, *370*(6518), 786–791. https://doi.org/10.1126/science.abb0971

23284277, 2025, 1, Downloaded from https://agupubs.onlinelibrary.wiley.com/doi/10.1029/2024EF005246 by Readcube (Labtiva Inc.), Wiley Online Library on [01/02/2025]. See the Terms and Conditions (https://onlinelibrary.wiley.com/terms-and-conditions) on Wiley Online Library for rules of use; OA articles are governed by the applicable Creative Commons License

Zander, K. K., Botzen, W. J. W., Oppermann, E., Kjellstrom, T., & Garnett, S. T. (2015). Heat stress causes substantial labour productivity loss in Australia. *Nature Climate Change*, *5*(7), 647–651. https://doi.org/10.1038/nclimate2623

Zhang, J., Zhang, K., Liu, J., & Ban-Weiss, G. (2016). Revisiting the climate impacts of cool roofs around the globe using an Earth system model. *Environmental Research Letters*, *11*(8), 084014. https://doi.org/10.1088/1748-9326/11/8/084014

Zhang, K., Cao, C., Chu, H., Zhao, L., Zhao, J., & Lee, X. (2023). Increased heat risk in wet climate induced by urban humid heat. *Nature*, *617*(7962), 738–742. https://doi.org/10.1038/s41586-023-05911-1

Zhang, K., Zhao, L., Oleson, K., Li, X., & Lee, X. (2024). Enhancing urban thermal environment and energy sustainability with temperature-adaptive radiative roofs [Dataset]. *Figshare*. https://doi.org/10.6084/m9.figshare.26264063.v1

Zhao, D., Aili, A., Zhai, Y., Xu, S., Tan, G., Yin, X., & Yang, R. (2019). Radiative sky cooling: Fundamental principles, materials, and applications. *Applied Physics Reviews*, *6*(2). https://doi.org/10.1063/1.5087281

Zhao, L., Lee, X., Smith, R. B., & Oleson, K. (2014). Strong contributions of local background climate to urban heat islands. *Nature*, *511*(7508), 216–219. https://doi.org/10.1038/nature13462

Zhao, Q., Guo, Y., Ye, T., Gasparrini, A., Tong, S., Overcenco, A., et al. (2021). Global, regional, and national burden of mortality associated with non-optimal ambient temperatures from 2000 to 2019: A three-stage modelling study. *The Lancet Planetary Health*, *5*(7), 415–425. https://doi.org/10.1016/S2542-5196(21)00081-4

References From the Supporting Information

IPCC. (2021). *Climate change 2021: The physical science basis. Contribution of working group I to the sixth assessment report of the intergovernmental panel on climate change*. Cambridge University Press. https://doi.org/10.1017/9781009157896

23284277, 2025, 1, Downloaded from https://agupubs.onlinelibrary.wiley.com/doi/10.1029/2024EF005246 by Readcube (Labtiva Inc.), Wiley Online Library on [01/02/2025]. See the Terms and Conditions (https://onlinelibrary.wiley.com/terms-and-conditions) on Wiley Online Library for rules of use; OA articles are governed by the applicable Creative Commons License